TFA

ACTA FACULTATIS TECHNICAE

TECHNICAL UNIVERSITY IN ZVOLEN

2

ISSUE: XXX ZVOLEN 2025

Medzinárodný zbor recenzentov / International Reviewers Board

TABLE OF CONTENTS

SCIENTIFIC PAPERS

SCIENTIFIC PAPERS

DESIGN AND EXPERIMENTAL EVALUATION OF ELECTRICAL PARAMETERS OF SMALL WIND GENERATOR

KONŠTRUKCIA A EXPERIMENTÁLNE HODNOTENIE ELEKTRICKÝCH PARAMETROV MALÉHO VETERNÉHO GENERÁTORA

Peter Koleda, Peter Hadžega

Department of Manufacturing and Automation Technology, Faculty of Technology, Technical University in Zvolen, T. G. Masaryka 54, 960 01 Zvolen, Slovakia, peter.koleda@tuzvo.sk

ABSTRACT: This paper presents the design and experimental verification of a small wind generator employing a levitation-based rotor support. The mechanical and electrical components of the system are described, with power generation based on the principle of electromagnetic induction – specifically, the induction of voltage in a conductor resulting from temporal changes in the magnetic field. The magnetic bearing of the rotor enables a significant reduction in mechanical friction, thereby improving the overall system efficiency. Experimental results confirm the agreement between the measured and theoretically calculated frequencies of the generated voltage, derived from the rotor speed and the number of magnetic poles. The study also includes an analysis of the induced voltage magnitude in individual stator windings. Finally, potential optimization approaches and future research directions for small wind generators with magnetic bearing systems are discussed.

Key words: renewable resources, wind generator, magnetic bearing system, induced voltage

ABSTRAKT: Tento článok prezentuje návrh a experimentálne overenie funkčnosti malého veterného generátora využívajúceho levitačný princíp uloženia rotora. Opísané sú konštrukčné riešenia mechanickej a elektrickej časti zariadenia, pričom výroba elektrickej energie je založená na princípe elektromagnetickej indukcie, teda na indukcii napätia vo vodiči v dôsledku časovej zmeny magnetického poľa. Magnetické uloženie rotora umožňuje výrazné zníženie mechanického trenia a tým prispieva k zvýšeniu účinnosti systému. Experimentálne výsledky potvrdzujú zhodu medzi nameranou a teoreticky vypočítanou frekvenciou generovaného napätia, odvodenou z otáčok rotora a počtu magnetických pólov. Súčasťou článku je aj analýza veľkosti indukovaného napätia na jednotlivých statorových vinutiach. V závere sú diskutované možnosti optimalizácie konštrukcie a smerovanie ďalšieho výskumu v oblasti malých veterných generátorov s magnetickým uložením.

Kľúčové slová: obnoviteľné zdroje, veterný generátor, magnetické uloženie, indukované napätie

INTRODUCTION

Decentralized electricity production through small wind turbines is a key element of local energy, island systems and strengthening the energy resilience of communities. According to the IEC 61400 family of standards, “small” turbines are generally considered to be those with a rotor area of less than 200 m^2 and a nominal voltage of up to 1,000 V AC or 1,500 V DC. The standard also specifies load classes and safety requirements for the design, installation and operation of these devices (International Electrotechnical Commission [IEC], 2020, 2019, 2022).

Compared to large onshore or offshore wind farms, small wind turbines are designed for local use of wind resources, often in rural environments with open wind flow, but also in built-up environments (buildings, roofs, masts). The key technical limitations are low to medium wind speeds and high turbulence, which reduce power utilization and increase fatigue loads. Recent eddy current simulations and experiments confirm that the breakdown of speed and turbulence structures at start-up fundamentally affects the power curve and dynamic

stresses; therefore, site selection and aerodynamic optimization are critical even for small generators (Jézéquel et al., 2024, Abkar and Porté-Agel 2015).

In terms of rotor typology, the principles of horizontal-axis wind turbines (HAWT) and vertical-axis wind turbines (VAWT) are applied in small wind simulators. In urban and suburban conditions, VAWTs are often investigated for their better resistance to turbulent and changing flows. Current studies show that a certain level of turbulence can even slightly improve the average power output and promote self-starting, although the effects are limited and sensitive to the geometry and distances between turbines (Yang et al., 2024, Al-Rawajfeh and Gooma 2023). A broader review of micro- to small-scale wind technologies and their integration into buildings points to the potential, but also to persistent limits in wind field estimation, interactions with buildings and capacity factors (Calautit and Johnstone 2023).

The theoretical maximum efficiency for axial turbines is given by the Betz limit (~59%) (Betz 1966, Arif 2019); real aerodynamic and electro-mechanical losses lead to a lower actual ratio of captured energy. The capacity factor for low winds is highly dependent on local conditions; for onshore turbines, a wide dispersion is generally reported in the literature (about 9 – 53% depending on location and design), while in built-up environments at low winds the capacity tends to be at the lower end of this range due to low speeds and increased turbulence (Center for Sustainable Systems 2024).

The aim of the article is to design a small experimental wind generator based on the levitation principle and verify its functionality by measuring the induced current in the stator winding.

MATERIAL AND METHODS

The experimental wind generator converts the kinetic energy of the air flow into electrical energy by using electromagnetic induction in the stator coils. Its structural assembly was designed in SolidWorks and is shown in Fig. 1. The functional model is shown in Fig. 2.

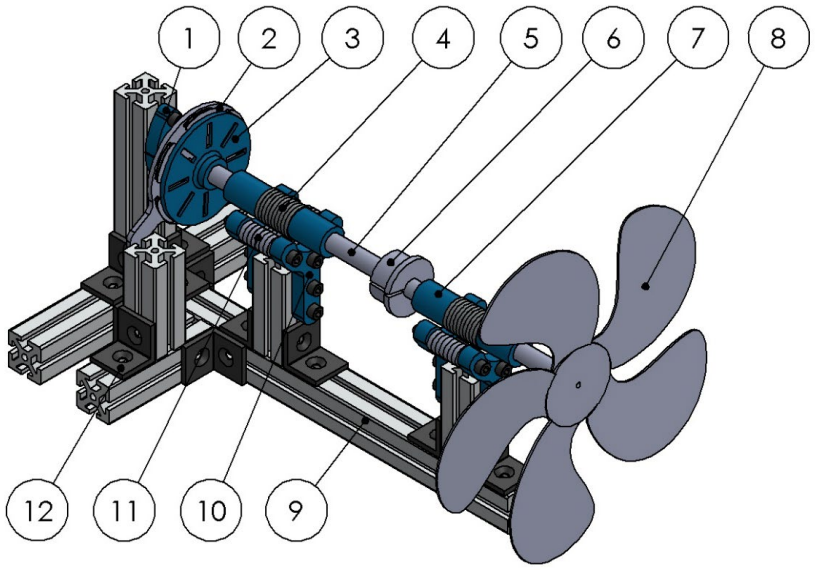

Fig. 1 Assembly of wind generator
Obr.1 Zostava veterného generátora

1 – centring part, 2 – stator with 6 coils, 3 – rotor with 8 neodymium magnets M1 with dimensions of 30 × 10 × 2 mm, 4 – circular neodymium magnets M2 with dimensions of Ø 32 × 18 × 4 mm, 5 – shaft, 6 – weight, 7 – case, 8 – propeller, 9 – frame from aluminium profile 40 × 40 mm, 10 – Y-shaped holder of magnets M3, 11 – circular neodymium magnets M3 with dimensions of Ø 20 × 8 × 5 mm, 12 – aluminium L profile 40 × 40 mm

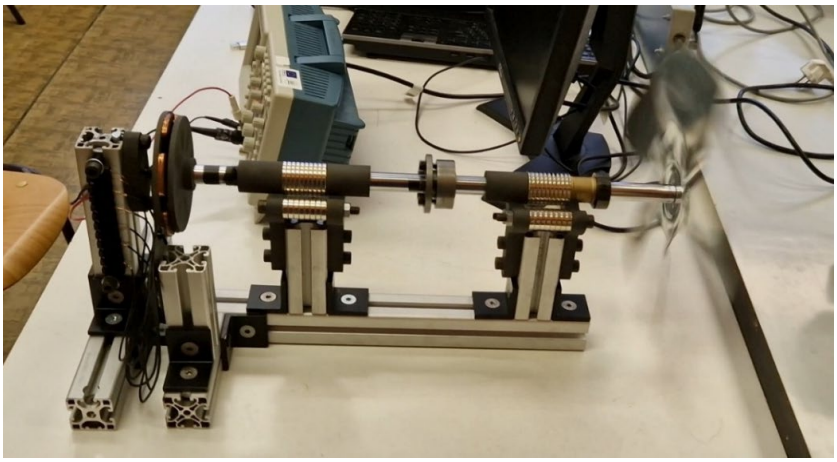

Fig. 2 Wind generator
Obr. 2 Veterný generátor

The device consists of a rotor (3) containing eight neodymium magnets M1 type N42 with dimensions of 30 × 10 × 2 mm, with a pull-out force of approximately 2.6 kg per magnet. These magnets are evenly distributed in a circle, creating a symmetrical magnetic field necessary for inducing voltage in the stator coils (2).

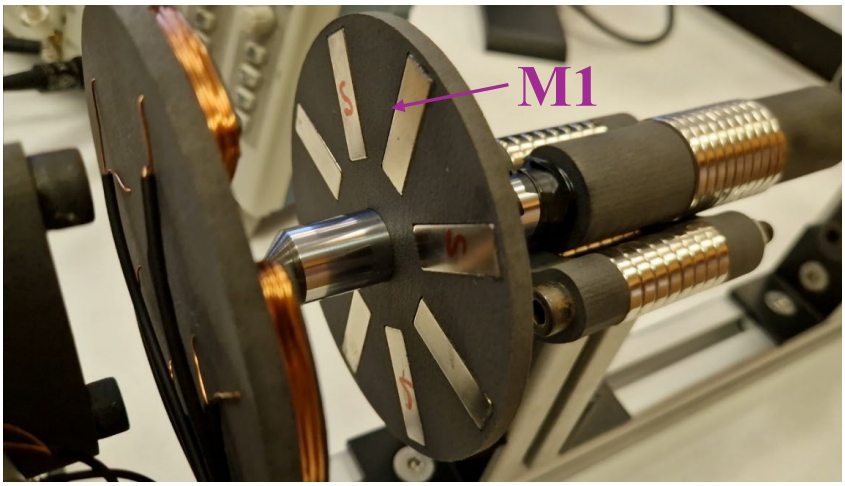

Fig. 3 Detail of rotor with eight permanent magnets M1
Obr. 3 Detail rotora s ôsmimi permanentnými magnetmi M1

The stator part is connected to the frame with screws and consists of six copper coils (Fig. 4), each of which contains 25 turns of coil wire Ø 0.50 mm (cross-section 0.196 mm²). The coils are positioned so that the magnetic lines of force of rotating magnet periodically intersect the coils, which leads to the induction of an electric current according to Faraday's law.

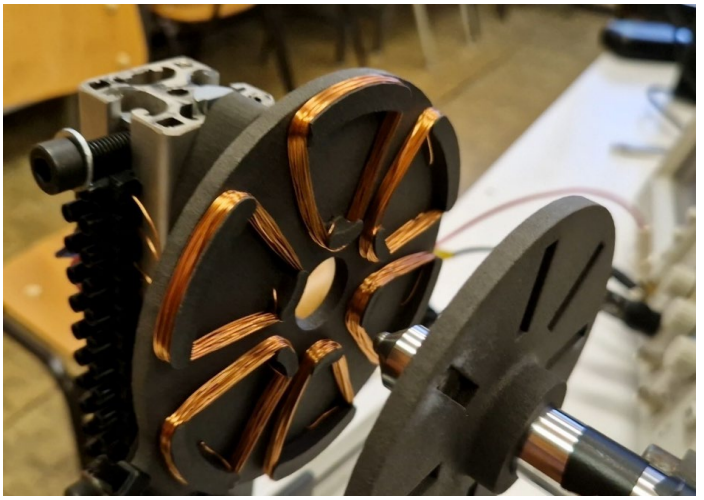

Fig. 4 Detail of stator with six copper coils
Obr. 4 Detail statora so šiestimi medenými cievkami

One of the design elements of the generator is the use of a levitation system (Fig. 5), which minimize friction. The rotor shaft is equipped with two groups of 10 circular neodymium magnets M2 (type N38) with dimensions of Ø 32 × 18 mm and a height of 4 mm, with a tear-off force of approximately 7.5 kg. These are mounted on supporting neodymium magnets M3 (type N38) in the number of 6 × 8 pcs and dimensions Ø 20 × 8 mm, height 5 mm, with a tear-off force of approximately 6.3 kg. By magnetic repulsion, the rotor shaft floats between these rows of magnets, which allows smooth rotation almost without mechanical contact. The rotor shaft is also driven by a propeller that uses air flow as a renewable energy source.

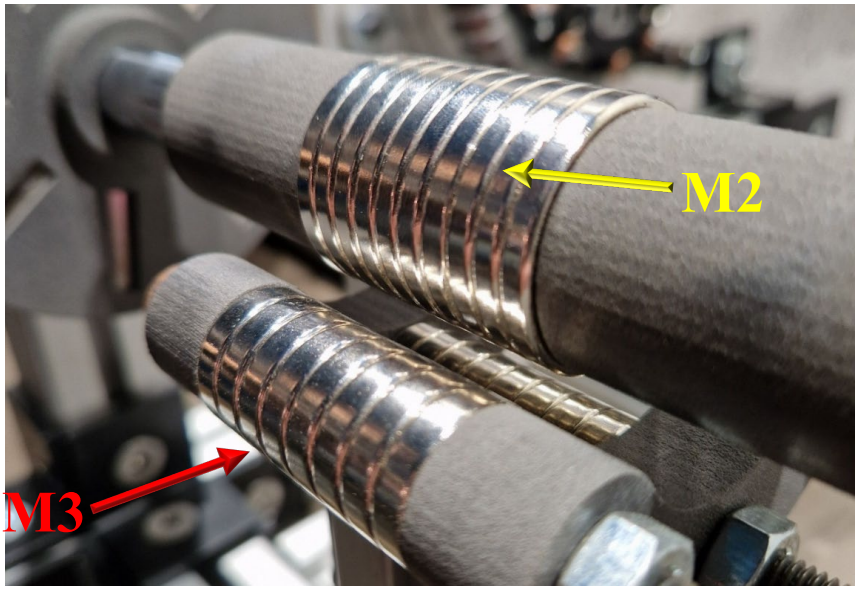

Fig. 5 Detail of magnetic bearing of generator
Obr. 5 Detail magnetického ložiska generátora

Another element of the magnetic guide is the centring part (Fig. 6) fitted on the inside with a neodymium magnet M4 Ø 10 × 10 mm, type N42, with a tear-off force of approximately 3.9 kg, which stabilizes the shaft tip in the desired position. The part is also shaped with a radius R150, which ensures automatic centring of the shaft during its operation (rotation). The shaft tip has a tip turned to a radius R6. The magnetic guide created in this way not only keeps the rotor in the axis but also maintains low friction.

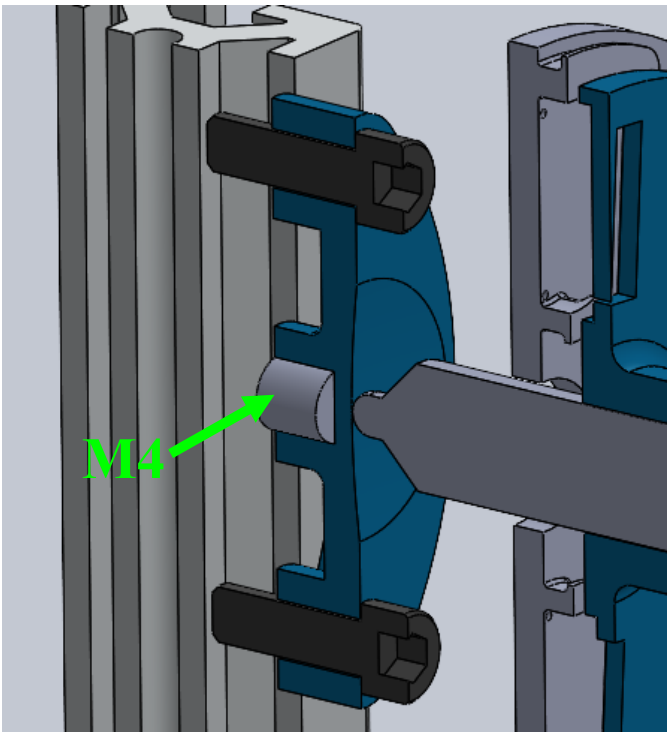

Fig. 6 Cross section of the centering part with magnet Ø 10 × 10 mm
Obr. 6 Prierez strediacim dielom s magnetom Ø 10 × 10 mm

The generator construction was designed with an emphasis on simplicity, modularity and low weight. The generator frame was made of 40 × 40 mm aluminium structural profiles, which ensure sufficient strength while allowing flexibility in assembling, expanding or modifying the generator set.

All key structural elements of the generator, including the rotor, stator, and Y-shaped magnet holders, were designed in 3D SolidWorks software. These parts were then manufactured on a powder 3D printer Formlabs fuse 1, which is designed for precise and efficient printing of functional parts from plastic powder (SLS technology), enabling high levels of accuracy, individual shape customization, and rapid prototyping.

The individual parts, such as the stator base, magnet holders and support brackets, were then firmly attached to the frame made of aluminium profiles using screw connections. This method of attachment ensures sufficient stability during operation, while also facilitating the disassembly or replacement of individual components during system testing and tuning.

The rotor part with permanent magnets and pressed-in bushings was firmly mounted on the generator shaft. This ensured mechanical stability, alignment and smooth movement during rotation, which is essential for the efficient conversion of mechanical into electrical energy through electromagnetic induction.

Theoretical calculation of induced voltage for the designed wind generator

In the plane of a sinusoidal waveform, according to Faraday's law, the amplitude of the voltage generated on the coil when the magnetic flux changes is:

$$\varepsilon_{peak} = N\frac{d\Phi}{dt}\ [\mathrm{V}], \tag{1}$$

where Φ is magnetic flux (V.s), N is number of turns.
For harmonic signal with frequency f and angular frequency $\omega = 2\pi f$ it can be written:

$$E_{peak} = N\,AB\omega \text{ [V]}, \quad (2)$$

where A [m^2] is coil conductor cross-section, B [T] is magnetic induction.

Used parameters for computation of generated voltage in one coil are in table 1.

Table 1 Parameters of computation for one generator coil
Tabuľka 1 Parametre výpočtu pre jednu cievku generátora

Parameter	**Value**
Number of threads N [-]	25
Coil conductor cross-section A [m^2]	2,56 . 10^{-5}
Assumed induction B in the working gap for a magnet of type N42 [T]	0,7
Revolutions n [RPM]	400
Number of coil pairs p [-]	4

Electric frequency of signal can be computed by term:

$$f_e = p \times f_m = 4 \times 6{,}667 \approx 26{,}6 \text{ Hz}, \quad (3)$$

where, p are pole pairs and f_m [Hz] is mechanical frequency of rotor rotations:

$$f_m = \frac{n}{60} = \frac{400}{60} = 6{,}667 \text{ Hz}. \quad (4)$$

Angular frequency of rotor can be computed as:

$$\omega = 2\pi f_e \approx 167{,}6 \text{ rad.s}^{-1}. \quad (5)$$

By substitution into (2), the amplitude of inducted voltage in winding is:

$$E_{peak} = 25 \times 2{,}56 \times 10^{-5} \times 0{,}7 \times 167{,}6 \approx 0{,}165 \text{ V} \quad (6)$$

and RMS value:

$$E_{rms} = \frac{E_{peak}}{\sqrt{2}} \approx \frac{0{,}165}{1{,}414} \approx 0{,}117 \text{ V}. \quad (7)$$

RESULTS AND DISCUSSION

To verify the functionality of the assembled generator, a workstation was assembled as shown in Fig. 7. A turbocharger with a Hitachi SJ200 frequency converter was used to spin the rotor using a stable air flow, due to the possibility of setting the required speed. Measurements were made at the output of one phase of the stator using a two-channel oscilloscope Tektronix TDS 2002B.

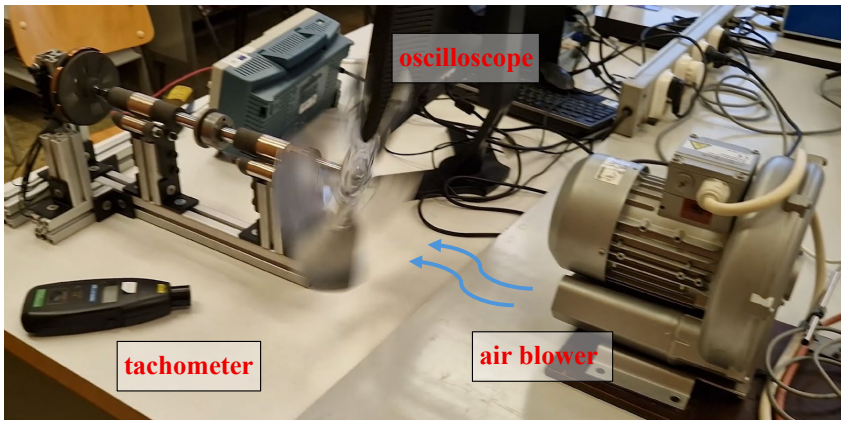

Fig. 7 Laboratory equipment with generator and oscilloscope
Obr. 7 Laboratórne pracovisko s generátorom a osciloskopom

Fig. 8 shows the voltage waveform at a rotor speed of 400 min^{-1}. The measurement parameters read from the measured waveform are summarized in Table 2.

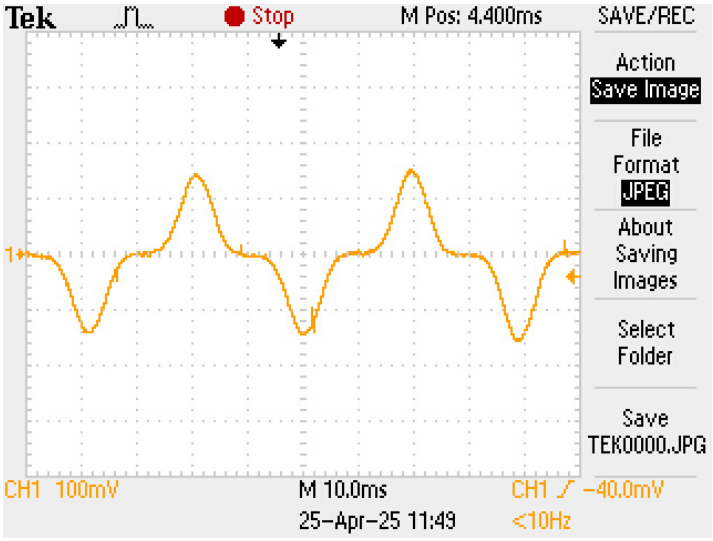

Fig. 8 The result of measuring the generator voltage on an oscilloscope Tektronix TDS 2002B (CH1: 100 mV, Timebase: 10 ms)
Obr. 8 Výsledok merania napätia generátora na osciloskope Tektronix TDS 2002B (CH1: 100 mV, časová základňa: 10 ms)

Table 2 Parameters of experimental measurement
Tab. 2 Parametre experimentálneho merania

Parameter	**Value**
Mechanical revolutions	400 min^{-1}
Number of coil pairs	8 poles (4 pairs)
Number of stator coils	6 coils
Vertical scale	100 mV
Horizontal scale	10 ms
Peak voltage	± 150 mV
Signal shape	Sinusoidal-pulsed with gentle overshoot

According to Faraday's law, the amplitude of the induced voltage E_{peak} is expressed by the equation (2) and by substituting it into the equation (6), its value is 0.165 V and the RMS value (7) is 0.117 V. Fig. 18 shows the measured waveforms and values, which confirm that E_{peak} is approximately 0.14 – 0.16 V and E_{rms} is 0.10 – 0.11 V. The slight deviation between the expected and measured voltage from the oscilloscope measurement can be caused by the gap between the rotor and stator of the generator where the value of magnetic induction B = 0.7 T is probably smaller.

The mechanical frequency of rotation is calculated as:

$$f_m = \frac{400\text{min}-1}{60} \approx 6{,}66 \text{ Hz} \tag{8}$$

and in combination with 4 electric pairs, it produces voltage with frequency

$$f_e = f_m \times p \approx 6{,}66 \times 4 = 26{,}66 \text{ Hz}, \tag{9}$$

what is a periodic cycle ≈ 37,7 ms (≈ 3,8 div at 10 ms/div).

If we consider that one "transition" between positive and negative peaks (half-period) lasts ≈ 20 ms, then it can be calculated:

$$f_{trans} = \frac{1}{T} = \frac{1}{0{,}02s} = 50 \text{ Hz}. \tag{10}$$

Measured mechanical frequency of rotor rotation is

$$f_{mech} = f_m \times 8 \approx 6{,}66 \times 8 = 53{,}28 \text{ Hz}. \tag{11}$$

The difference between the theoretical frequency 50 Hz and the measured 53.28 Hz is caused by the inaccuracy of the oscilloscope time base reading and the rotor speed fluctuations. For a complete AC voltage cycle (full period) then:

$$f_{cycle} = \frac{f_{trans}}{2} \approx \frac{53{,}28}{2} = 26{,}64 \text{ Hz}, \tag{12}$$

where:

f_m is mechanical frequency of rotor revolutions [Hz], f_e is electric frequency of induced voltage [Hz], p is number of coil pairs, T is half period [s], f_{trans} is frequency of transition between positive and negative peak voltage [Hz], f_{cycle} is frequency of full period [Hz].

The shape of the signal course shows:

1. Rapid voltage rise as the pole passes through the centre of the coil.
2. Oscillatory reverberation when crossing zero coupling – a consequence of the resonance of the winding system and parasitic capacitances.

3. Symmetrical positive and negative maxima, which confirms the correct balance of the magnetic field and the correspondence of the revolutions with the theoretical design.

These results confirm that the generator design with eight magnets on the rotor and six coils on the stator delivers a stable AC signal with a spectrum suitable for low-speed wind applications.

CONCLUSION

A model of a wind generator was designed and manufactured, the main elements of which are a rotor with eight neodymium magnets, a stator with six copper coils and magnetic bearings. These components enable contactless and almost lossless transfer of mechanical energy to electrical energy, while the resulting alternating current can be further analysed using the designed laboratory measuring station.

Testing of the generator demonstrated its functionality and confirmed the validity of the physical assumptions based on Faraday's law of electromagnetic induction. Measurements showed that at a rotor speed of 400 min^{-1} (≈ 6.66 Hz) the generator produced an average output voltage with an amplitude of ±150 mV, which differs only minimally from the theoretical calculation of 165 mV, and an electrical frequency of approximately 26.5 Hz, which corresponds to the theoretical calculation for four electrical pairs of poles (8 polarity transitions per revolution). The measured half-cycle transitions lasted approximately 20 ms (≈ 53 Hz), with a negligible deviation from the calculated 50 Hz caused by the inaccuracy of the time base reading and speed fluctuations.

The identified technical shortcomings, such as the limited stabilization angle of the rotor or the absence of directional turning according to the wind, provide possibilities for further development and optimization of the device. The proposed solutions may contribute to the creation of an efficient low-cost system for generating electricity for remote areas in the future.

ACKNOWLEDGMENT

This research was funded by APVV-20-0403 „FMA analysis of potential signals suitable for adaptive control of nesting strategies for milling wood-based agglomerates“ and the EU NextGenerationEU through the Recovery and Resilience Plan for Slovakia under project No. 09I03-03-V05-00016.

REFERENCES

ABKAR, M. AND PORTÉ-AGEL, F. 2015. Influence of atmospheric stability on wind-turbine wakes: A large-eddy simulation study. *Phys. Fluids*, 27, 035104, https://doi.org/10.1063/1.4913695

AL-RAWAJFEH, M.A., GOOMA, M.R. 2023. Comparison between horizontal and vertical axis wind turbine. *International Journal of Applied Power Engineering* vol. 12 no. 1 DOI: 10.11591/ijape.v12.i1.pp13-23

ARIF, M. 2019. Power Generation Technologies: An Introduction. Islamabad: Pakistan Institute of Engineering and Applied Sciences (PIEAS). p. 178. ISBN 978-969-7583-01-0.

BETZ, A. 1966. Introduction to the Theory of Flow Machines. (D. G. Randall, Trans.) Oxford: Pergamon Press.

CALAUTIT, K., JOHNSTONE, C. 2023. State-of-the-art review of micro to small-scale wind energy harvesting technologies for building integration, *Energy Conversion and Management*: X, Vol. 20, p. 100457, ISSN 2590-1745. https://doi.org/10.1016/j.ecmx.2023.100457.

Center for Sustainable Systems, University of Michigan. 2024. "Wind Energy Factsheet." Pub. No. CSS07-09.

International Electrotechnical Commission. (2020). *IEC 61400-2: Wind energy generation systems – Part 2: Small wind turbines*.

International Electrotechnical Commission. (2019). *IEC 61400-11: Wind turbine generator systems – Part 11: Acoustic noise measurement techniques*

International Electrotechnical Commission. (2022). *IEC 61400-12-1: Wind energy generation systems – Part 12-1: Power performance measurements of electricity producing wind turbines*.

JÉZÉQUEL, E., BLONDEL, F., MASSON, V. 2024. Breakdown of the velocity and turbulence in the wake of a wind turbine – Part 1: Large-eddy-simulation study, *Wind Energ. Sci*., 9, 97–117, https://doi.org/10.5194/wes-9-97-2024.

YANG, Y., CAO, Y., QIAN, Z., WANG, J., ZHU, Y., CHEN, X., ZHANG, W., WANG, Y., WU, G., CHEN, S. 2024. A Study on the Effect of Turbulence Intensity on Dual Vertical-Axis Wind Turbine Aerodynamic Performance. *Energies*, *17*(16), 4124. https://doi.org/10.3390/en17164124

Corresponding author:
Peter Koleda, xkoledap@is.tuzvo.sk

CCT DIAGRAMS FOR SINTERHARDENING OF PM CHROMIUM-MOLYBDENUM MASTER ALLOY STEELS WITH HYBRID ALLOYING POWDERS

CCT DIAGRAMY PRE SINTERHARDENING PM CHROM-MOLYBDÉNOVÝCH PREDLEGOVANÝCH OCELÍ S HYBRID-NÝMI LEGUJÚCIMI PRÁŠKAMI

Dmitriy Koblik[1], Miroslava Ťavodová[2],

[1] *Faculty of Technology, Technical University in Zvolen. Študentská ulica 26, 960 01 Zvolen, Slovakia. E-mail: dmitriy.koblik@gevorkyan.sk*

[2]*Faculty of Technology, Technical University in Zvolen. Študentská ulica 26, 960 01 Zvolen, Slovakia. E-mail: tavodova@tuzvo.sk*

ABSTRACT: The article reviews the possibilities of introducing alloying elements into the material formed by powder metallurgy, in order to adjust the alloying element content. There are several methods in powder metallurgy (PM) and each alloying method has its advantages and disadvantages. Master alloys (MA), powders with a high content of typically several alloying elements, can be added in small amounts to the base powder, especially to introduce oxygen-sensitive elements such as Cr, Mn and Si. In addition, Master alloys can be designed to form a liquid phase during the sintering process. This will ensure an improved distribution of the alloying elements in the material and thus accelerate homogenization. In this study, such MAs were combined with pre-alloyed Cr-Mo base powders to form hybrid alloy mixtures with the aim of improving the hardenability of the material during sinterhardening. The hybrid alloys were compared with mixtures of MA and pure iron as a reference material. The hardenability during sinterhardening of all materials was determined by creating Continuous Cooling Transformation (CCT) diagrams recorded with different cooling rates.

Key words: sinterhardening, sintering, prealloyed material, master alloy (MA), cooling rate, CCT diagram

ABSTRAKT: Článok sa zaoberá prehľadom možností zavadzania legujúcich prvkov do materiálu, vytvoreného práškovou metalugiou, s cieľom upraviť obsah legujúcich prvkov. V práškovej metalurgii (PM) existuje niekoľko spôsobov a každý spôsob legovania má svoje výhody a nevýhody. Master alloys (MA), prášky s vysokým obsahom typicky niekoľkých legujúcich prvkov sa môžu pridávať v malých množstvách do základného prášku, najmä na zavedenie prvkov citlivých na kyslík, ako sú Cr, Mn a Si. Okrem toho môže byť Master alloys navrhnuté tak, aby sa počas procesu spekania vytvorila kvapalná fáza. To zabezpečí zlepšenie rozloženia legujúcich prvkov v materiáli a urýchlili sa tak homogenizácia. V tejto štúdii boli takéto MA kombinované s predlegovanými základnými práškami Cr-Mo za účelom vytvorenia hybridných legovaných zmesi s cieľom zlepšiť kaliteľnosť materiálu počas sinterhardeningu. Hybridné zliatiny boli porovnávané so zmesami MA a čistého železa ako referenčného materiálu. Kaliteľnosť počas sinterhardeningu všetkých materiálov bola stanovená vytvorením Continuous Cooling Transformation (CCT) diagramov zaznamenaných s rôznymi rýchlosťami chladenia.

Kľúčové slová: sinterhardening, spekanie, predlegovaný materiál, master alloy (MA), rýchlosť chladenia, CCT diagram

INTRODUCTION

Industrial trends over the past decade have significantly increased the demands on mass production of parts, especially in the automotive industry. Cost reduction, high quality standards for millions of manufactured parts, such as high precision, mechanical properties, environmental requirements have contributed to the accelerated development of powder metallurgy. For the further expansion of PM into new industrial areas and applications, materials with improved properties are needed. One such method is the sinterhardening process. The sinterhardening process significantly simplifies the production of parts, as sintering and hardening are integrated into one cycle. This solution achieves the controlled formation of a

martensitic structure that occurs during cooling after sintering. As a result, hardness and mechanical properties are improved. The process uses special sintering furnaces in which a suitably designed controlled cooling zone is applied. This eliminates the need for a separate thermomechanical hardening process, eliminating the need to design additional operations and minimizing costs and production time (Engström, et al. 2020) (Kalss, et al. 2022).

Achieving high dimensional accuracy of components is another fundamental advantage of sinterhardening. Since the entire thermal transformation occurs within a single operation, the risk of thermal deformation and subsequent distortion of the part is significantly reduced. This accuracy is especially valued in areas where tolerances are crucial – for example, in the automotive, aerospace or military industries. In addition, automated process integration ensures consistency of the resulting properties of the parts, which is important from the point of view of the quality and reliability of the final products (Gábrišová, et al. 2019).

The energy efficiency of sinterhardening is another significant benefit. Compared to traditional methods, where separate heat treatments (such as superheating, rapid cooling, washing and subsequent tempering) are required, sinterhardening can reduce energy consumption by up to 60 %. Manipulating the temperature profile directly during sintering not only reduces energy consumption, but also the need for additional processing of parts, which also reduces operating costs. This environmentally friendly approach is also beneficial for manufacturers striving for more sustainable production (Krauss, 2015) (Kozový, et al. 2023).

The main limitation is the low cooling rate achieved during sinterhardening. In current industrial furnaces, cooling rates of 2-5 $K.sec^{-1}$ can be achieved. In addition, as shown by (Bocchini, 2002), the surface to volume ratio also plays an important role, since the heat transfer between the part and the atmosphere is a factor determining the cooling rate.

To compensate for the slow cooling compared to oil quenching, the alloying system must be adjusted accordingly, requiring a higher content of alloying elements. Special PM steel grades have been developed for sintering, for example based on pre-alloyed Fe-Mo powder with diffusion-bonded Cu or Cu + Ni (Engström, et al. 2002) (Karamchedu, et al. 2014).

These alloying elements are often used in PM because of their low affinity for oxygen. Therefore, any oxides in the pressings can be easily reduced during sintering and the risk of oxygen capture from the sintering atmosphere is also minimal. However, these elements are expensive and Ni is classified as carcinogenic, as some result elements such as Cr are increasingly considered advantageous, and Cr and Cr-Mo overalloyed powders are now commercially available at a reasonable price (Berg, Maroli, 2002). These powders have more precise requirements regarding the chemical composition and quality of the sintering atmosphere, but this is now manageable and it has been shown that this class of materials is also suitable for sintering, at least if the desired result is a martensitic structure. Carbon control is also essential for sintered steels and is more complex than for metallic steels, especially for sintered steels alloyed with elements with a high affinity for oxygen, such as Cr, Mn and Si, which makes carbon loss during sintering a key issue. This also applies to high-temperature sintering, when deoxidation is greater, but at the cost of higher carbon loss (Danninger, Giert, 2001).

Unlike metal parts, in PM, not only the choice of alloying elements but also the alloying method is a parameter that affects the properties of the final material. One way to add several alloying elements is to admix MA. MA is a powder with a high alloying element content, which usually contains several elements combined in one powder. It is a good way to supplement oxygen-sensitive elements such as Cr, Mn and Si. In addition, MA can be designed to form a liquid phase during the sintering process to improve the distribution of alloying elements in the material and to accelerate homogenization. Pre-alloyed powders show a homogeneous distribution of alloying elements, but due to solution hardening, the powders are harder and

therefore less compactable than pure elemental powders of each element (Kalss, 2007) (Mardan, M., Blais 2016). It has proven difficult to sinterharden steels from most prealloyed powders under standard conditions without the addition of additional alloying elements, except for powders with relatively high alloying element content, which multiplies the cost and the problem of pressing (Hoganas, 2017) Geroldinger 2021).

By implementing new automation techniques, such as high-pressure water atomization of powder, it is now possible to produce MA powders containing Fe, Si, C, Cr and Mn with low oxygen content (De oro Calderon, 2019) (Geroldinger, 2019).

MATERIAL AND METHODS

A discussion about the efficiency and performance possibilities of modern metal manufacturing is incomplete without the concept of sintering in powder metallurgy. Conventional sintering processes are the bread and butter of improving a part with PM. This process heats the compacted part to fuse the loosely bonded particles for improved strength and hardness. After sintering, the powder metal part is often heat treated by reheating to permit quenching and tempering. This further increases the hardness and strength of the compacted component (Gábrišová, et al. 2019). One advantage of powder metallurgy is the ability to sinter the part and then, thanks to controlled cooling, create a wide variety of strength and hardness combinations. At one end of this range is very slow cooling to create a soft magnetic part; the other extreme is effectively atmosphere quenching the part to form a martensitic structure with the same hardness as quenching - but without the additional processing (Knaislová, et al. 2017).

Out of several metal hardening process types, sinter hardening stands out. It combines the benefits of sintering and hardening into one operation. Secondary operations are minimized and greater dimensional accuracy is achieved.

Figure 1a shows characteristics of conventional sintering. Conventional sintering has greater flexibility in material selection, need to have secondary hardening operation (if required), potential of larger distortion due to heat treatment, ideal for DC magnetic properties.

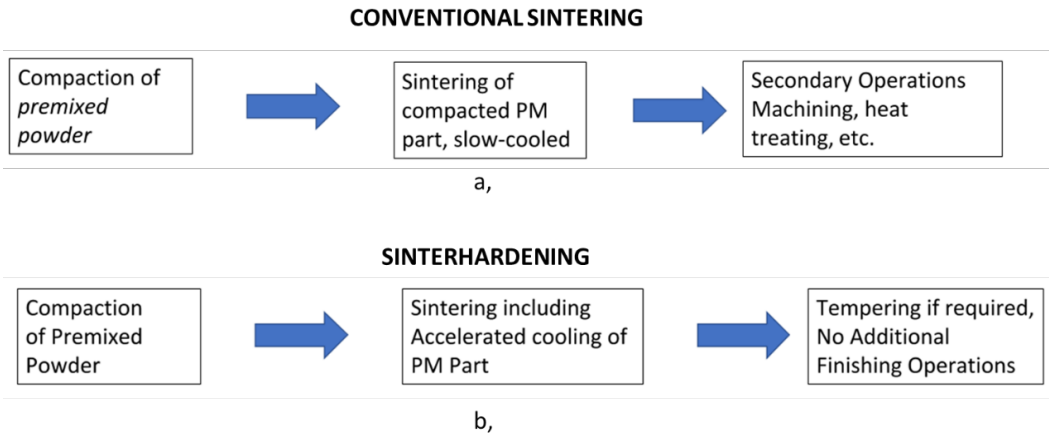

Figure 1 Conventional sintering processes (a,); sintering with the inclusion of heat treatment (b,)

Obrázok 1 Postupy konvenčného spekania (a,); spekanie so zaradením tepelného spracovania - sinterhardening (b,)

The Figure 1b shows characteristics of sinterhardening. The sinter hardening has heat treatment incorporated into sintering circle, reduced processing steps, greater dimensional precision, reduced material flexibility heat treatment incorporated into sintering circle, reduced processing steps, greater dimensional precision, reduced material flexibility.

Conventional heat treatment (reheating and quenching) forms martensite within the part that has high hardness but is quite brittle. Tempering lowers the hardness slightly but dramatically increases the strength. This has been the tried-and-true method for hardening in both PM and conventional parts manufacturing. However, using special sintering furnaces coupled with engineered powder materials creates the opportunity to eliminate the reheating step and merge it into the sintering step. This gives the same transformation along with the advantages of strength and hardness.

Sinterhardening allows for improved mechanical properties of parts. The resulting martensitic structure provides a combination of high hardness and wear resistance, which is especially important for components exposed to high mechanical stress. In addition, the optimized process ensures minimal variability of properties between individual products, which significantly contributes to the overall reliability and performance of the products.

The article presents the results of sinterhardening of materials ASC100.29, Astaloy85Mo, AstaloyCrA, AstaloyCrM and Astaloy CrS with MA addition. Alloying elements were measured using laser ablation mass spectrometry and inductively coupled plasma. Carbon content was determined by C-LECO measurements. For the measurement, the standard for steel pins was 501-679, with a content of 0.799±0.011 wt. % carbon. The powders were mixed in a Turbula mixer for 10 minutes according to the standard industrial procedure. Samples with dimensions of 10 x 7 x 4 mm were pressed at a pressure of 600 MPa and Multical calibration oil was used. The pressings were isothermally sintered at T=1 300 °C for 1 hour. under defined conditions in an electrically heated furnace with a gas-tight tubular retort under an atmosphere of high-purity argon and cooled to room temperature in the furnace outlet zone with water cooling at rates of 1.5 and 3.0 $K.sec^{-1}$.

The composition of the materials used is given in Table 1, the composition of the powder mixes is given in Table 2.

Table 1 Chemical composition of basic materials
Tabuľka 1 Zloženie základných materiálov

Basic material[1)]	Chemical composition of basic material[2)] [wt.%]					
	Fe	Si	Mn	Cr	Mo	C
ASC100.29	99.81	0.00	0.13	0.05	0.01	0.00
Astaloy85Mo	98.93	0.00	0.17	0.05	0.85	0.00
AstaloyCrA	98.01	0.03	0.13	1.80	0.03	0.00
AstaloyCrM	96.32	0.03	0.15	3.00	0.50	0.00
AstaloyCrS	98.82	0.03	0.15	0.85	0.15	0.00
H45	56.00	8.00	0.00	32.00	0.00	4.00
H46	48.00	6.00	42.00	0.00	0.00	4.00
H47	35.30	6.00	28.00	27.00	0.00	3.70
H166	56.10	7.50	33.00	0.00	0.00	3.4
H200	49.50	9.00	40.00	0.00	0.00	1.5

[1)]Základný materiál, [2)]Chemické zloženie základného materiálu

Table 2 Composition of powder mixes
Tabuľka 2 Zloženie práškových mixov

Powder mixes[1)]	Chemical composition of basic material[2)] [wt.%]					
	Fe	Si	Mn	Cr	Mo	C
ASC + 4%H45	97.89	0.39	0.13	1.09	0.01	0.49
ASC + 4%H46	97.83	0.21	1.46	0.05	0.01	0.44
ASC + 4%H47	97.49	0.32	0.88	0.82	0.01	0.48
Ast85Mo + 4%H45	96.89	0.38	0.17	1.24	0.83	0.49
Ast85Mo + 4%H46	97.23	0.24	1.23	0.05	0.81	0.44
Ast85Mo + 4%H47	96.50	0.34	0.94	0.91	0.82	0.49
AstCrA + 4%H45	96.31	0.47	0.13	2.60	0.03	0.46
AstCrA + 4%H46	96.15	0.31	1.44	1.65	0.03	0.42
AstCrA + 4%H47	95.45	0.44	1.03	2.58	0.03	0.47
AstCrM + 4%H45	95.01	0.44	0.15	3.49	0.47	0.44
AstCrM + 4%H46	94.91	0.28	1.07	2.87	0.48	0.39
AstCrM + 4%H47	94.26	0.45	0.91	3.48	0.46	0.44
Ast85Mo + 4%H166	96.39	0.32	1.44	0.03	0.84	0.69
Ast85Mo + 4%H200	96.34	0.35	1.72	0.02	0.86	0.71
AstCrS + 4%H166	96.53	0.31	1.45	0.84	0.13	0.74
AstCrS + 4%H200	96.20	0.36	1.73	0.85	0.13	0.73

[1)]Práškový mix, [2)]Chemické zloženie základného materiálu

RESULTS AND DISCUSSION

It is clear that the iron powder steels ASC100.29 and lower alloyed master alloys such as Astaloy85Mo and AstaloyCrA cannot be hardened by sinterhardening at industrially achievable cooling rates, at least at this carbon content. AstaloyCrM can form a martensitic microstructure without any additional alloying elements (Kalss, 2007) (Krauss, 2015). For all other steels it is clear that if martensitic hardening is desired at conventional sinterhardening cooling rates, additional alloying elements need to be added to the material.

Figure 2 shows the CCT diagrams of various base powders + 4% H45 (MA Cr-Si). These CCT diagrams are shown here as examples. Similar CCT diagrams were created with other base powder + MA combinations. Sintered steels made from ASC100.29 iron powder, at least with the carbon content chosen here, cannot be hardened under standard sintering conditions, even in combination with MA, with the exception of H47 (MA Mn-Cr-Si) (Geroldinger, 2019). In contrast, hybrid alloy powder mixtures can be hardened by sinterhardening at a cooling rate of 1.5 $K.sec^{-1}$, sometimes even lower. This means that at the carbon content considered in this study, pre-alloyed powders should be combined with MA powder (hybrid alloying) if a martensitic microstructure is desired. Although it is possible to achieve a martensitic microstructure with AstaloyCrM without MA, the combination with MA leads to even higher macro- and microhardness. The Figure 3d shows the CCT diagram of the hybrid powder mixture AstaloyCrM + 4% H45. It can be observed that at cooling rates of 1 $K.sec^{-1}$ and 0.75 $K.sec^{-1}$ pearlite formation occurs in the hybrid alloy material. The reason for

this finding is that the heat treatment at the investigated temperatures and times may not be sufficient to completely dissolve the carbides in the material, and therefore less dissolved carbon is available in the austenitic matrix than it should be nominally (Kozový, et al. 2023).

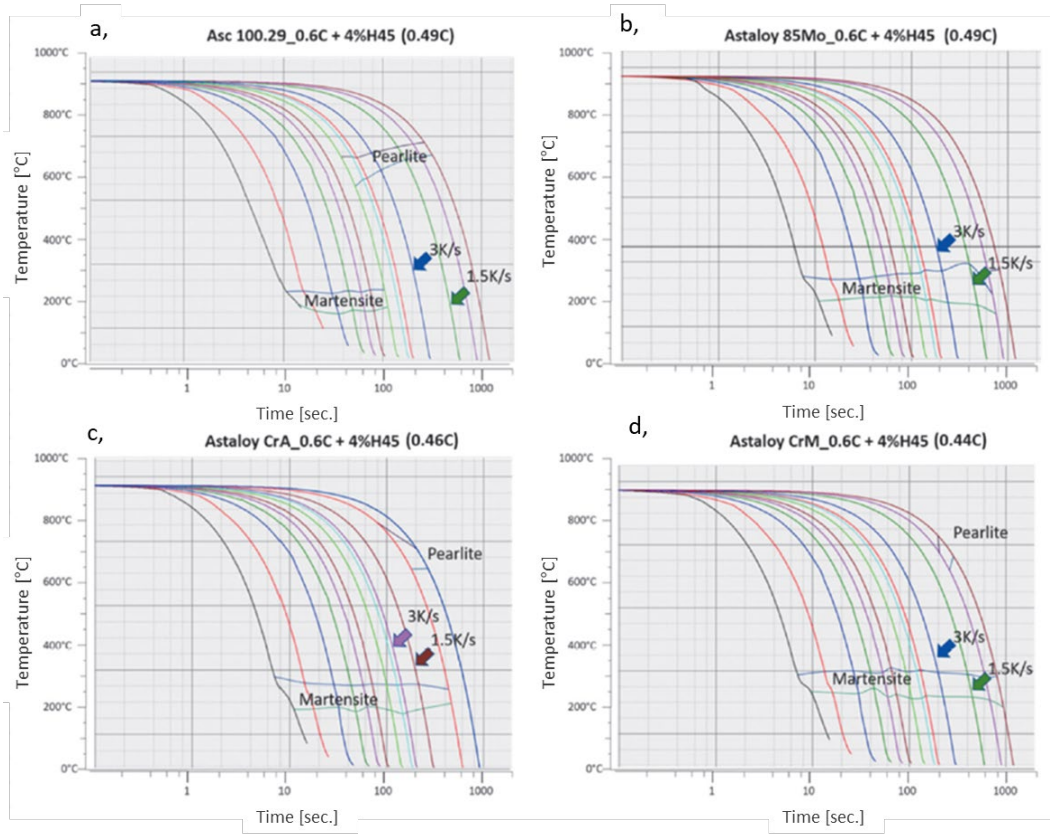

Figure 2 CCT diagram of powders obtained by mixing with 4%H45 (Geroldinger, 2019)
Obrázok 2 CCT diagram práškov, získaných mixom s 4%H45 (Geroldinger, 2019)

Regarding the combination of MA with Astaloy85Mo and AstaloyCrS, to characterize the sinterhardening and in particular to reliably estimate the effective cooling rates leading to martensitic microstructures, CCT diagrams were evaluated in a quenching dilatometer. These are shown in Figure 3 (Geroldinger et al, 2024), the transformations were identified from the cooling graphs. These diagrams clearly confirm that the pre-alloyed materials do not sinter and do not harden even at higher carbon levels; quenching would require cooling rates that are significantly higher than those possible in industrial furnaces. The addition of pre-alloyed MA drastically increases the hardenability: even at cooling rates as low as 1 $K.sec^{-1}$, no bainitic or pearlitic transformation is visible. This is in agreement with the relatively high hardness levels after sintering and the partially martensitic microstructures after sintering.

However, it should be considered that, as reported for example by (Geroldinger et al, 2021), small areas with bainitic or pearlitic transformation are not shown in the CCT diagram. Although the diagram predicts fully martensitic microstructures, metallography may reveal some pearlite or bainite, especially in the cores of the largest particles of the former base powder. In practice, the system tolerance is relevant in terms of cooling rate. For Astaloy85Mo-

MA-C, the CCT diagram indicates bainite at cooling rates <1 K.sec^{-1}. In this material, even the cores of the larger particles were sufficiently alloyed, leading to full martensitic transformation at 3 K.sec^{-1}.

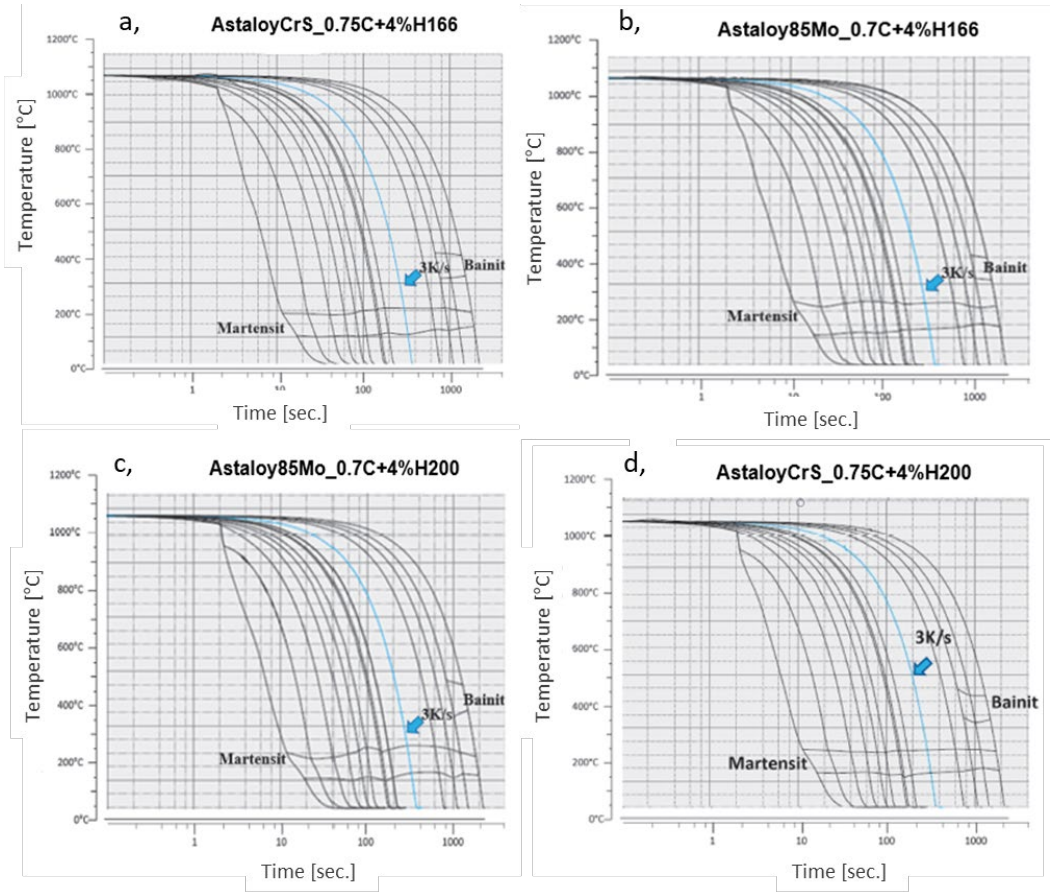

Figure 3 CCT diagram of powders obtained by mixing with 4%H200 (Geroldinger et al, 2024)

Obrázok 3 CCT diagram práškov, získaných mixom s 4%H200 (Geroldinger et al, 2024)

The admixture of master alloys has a high impact on the hardenability of the material, and, therefore, the mechanical and fatigue properties. This type of alloying is very promising for improving the properties of low-alloy steels (such as AstaloyCrS and AstaloyCrA) while maintaining a competitive price.

CONCLUSION

Sinterhardening combines the advantages of sintering and hardening into a single operation. Secondary operations are minimized and greater dimensional accuracy is achieved. The article presents the results of sinterhardening of the materials ASC100.29, Astaloy85Mo, AstaloyCrA, AstaloyCrM and Astaloy CrS with the addition of MA, as individual authors have investigated and published the results of experiments with powder mixes. Hybrid alloys were compared with mixtures of MA and a reference material - pure Fe. Hardenability during

sinterhardening of all materials was determined by creating Continuous Cooling Transformation (CCT) diagrams, recorded at different cooling rates.

We can summarize the results and conclude that the hybrid alloying technique, which means the combination of pre-alloyed powder and MA powder, significantly improves hardenability compared to steels made from pure iron powder. Martensitic hardening of pure Fe powder could be achieved at a rate of 3 $K.sec^{-1}$ and MA of the Fe-Mn-Cr-Si-C type. The use of a base powder pre-alloyed with 0.85% Mo in combination with MA leads to hybrid alloy mixtures with high hardness and good hardenability. Purely martensitic homogeneous microstructures can be achieved with all hybrid alloy materials using AstaloyCrM as the base powder. Materials based on AstaloyCrM show the smallest differences in hardness at cooling rates of 3 and 1.5 $K.sec^{-1}$.

ACKNOWLEDGMENT

This work was supported by Scientific Grant Agency of the Ministry of Education, science, research and sport of the Slovak Republic and the Slovak Academy of Sciences under the grant number VEGA 1/0073/24 „Experimental analysis of shapes and materials of working tools of additional equipment of forestry mechanization technology “.

REFERENCES

BOCCHINI, G.F., et al. 2002. Influence of density and surface/volume ratio on the cooling speed of sinter-hardening materials, Part two: Microstructure and microhardness distribution inside parallelepipeds. In *Adv. Powder Metall.&Patric. Mater*. – 2002, MPIF, Princeton NJ, Part13, 2002, p.60.

BERG, S., MAROLI, B. 2002. Properties obtained by chromium-containing material. In *Adv. Powder Metall.&Patric. Mater*. – 2002, MPIF, Princeton NJ, Part 8, 2002, p.1.

DANNINGER, H., GIERT, C. 2021. Processes in PM steel compacts during the initial stages of sintering, In *Mater. Chem. Physics*. 67 (2001) 1, pp. 49-55, DOI:0.1016/S0254-0584(00)00419-3.

DE ORO CALDERON, R., DUNKLEY, J., GIERL, C., DANNINGER, H. 2019. New opportunities for master alloys: Ultra-high pressure water atomized powders. In *Powder Metall. Review 8* (2019) 1, pp. 55-66.

ENGSTRÖM, U., MC. LELLAND, J., MAROLI, B. 2002. Effect of sinter hardening on the properties of high temperature sintered PM steels. In *Adv. Powder Metall.* & *Partic. Mater*. MPIF, Princeton NJ, Part 13, 2002, p. 1.

GÁBRIŠOVÁ, Z., BRUSILOVÁ, A., ŠVEC, P. 2019. Study of Sintering Parameters and Sintering Additives

GEROLDINGER, S. 2019. Optimization of iron-based Master Alloys for liquid phase sintering of PM steels. Master Thesis, TU Wien, 2019.

GEROLDINGER, S., DE ORO CALDERON, R., GIERTL-MAYER, C., DANNINGER, H. 2021. Sinter hardening PM steels prepared through hybrid alloying, In *HTM J.Heat. Treatm. Mat.* 76 (2021) 2; pp. 105-119, DOI:10.1515/htm-2020-0007, open access.

GEROLDINGER, S., HOJATI, M., DE ORO CALDERON, R, GIERTL-MAYER, C., DANNINGER, H., HELLEIN, R. 2024. Hybrid alloyed sinter hardening steels based on different prealloyed powders. In J. *Heat. Treatm. Mat*. 79, 3; pp. 147-158.

HOGANAS 2017. Iron and steel powders of sintered components. Hoganas Handbook for sintered components. Hoganas, Sweden, 2017. ISBN:978-91-983614-0-7.

KALSS, G. 2007. Sinterhärten von Cr-Mo-legierten PM-Stählen fur hochbelastbare Präzisionsteile, Dissertation, TU Wien, 2007, p.321.

KALSS, G., GIERL-MAYER, CH., DANNINGER, H., STETINA, G. 2022. Sinter Hardening of Cr-Mo Pre-Alloyed Steels as a Function of the Carbon Content. In *Powder Metallurgy Progress*. Vol. 20, No. 2, Slovak Academy of Sciences, 2020, pp. 81-93. https://doi.org/10.2478/pmp-2020-0008

KARAMCHEDU, S., HATAMI, S., NYBORG, L., ANDERSSON, M. 2014. Sinter-hardening response of sintered steel based on Astaloy Mo and its diffusion bonded derivatives In *Powder Metallurgy Progress,* vol.14, no.2, 2014, p.93.

KNAISLOVÁ, A., ŠIMŮNKOVÁ, V., NOVÁK, P., PRŮŠA, F., CYGAN, S., JAWORSKA, L. 2017. The Optimization of Sintering Conditions for the Preparation of Ti-Al-Si Alloys. In *Manufacturing Technology.* 2017;17(4):483-488. doi: 10.21062/ujep/x.2017/a/1213-2489/MT/17/4/483.

KOZOVÝ, P., ŠAJGALÍK, M., DRBÚL, M., HOLUBJÁK, J., MARKOVIČ, J., JOCH, R., BALŠIANKA, R. 2023. Identification of Residual Stresses after Machining a Gearwheel Made by Sintering Metal Powder. In *Manufacturing Technology*. 23(4):468-474. doi: 10.21062/mft.2023.054.

KRAUSS, G. 2015. Steels: processing, structure and performance. ASM International, Ohio, 2015, p.705. - ISBN: 978-0871708175.

MARDAN, M., BLAIS, C. 2016. Development of Novel of Pre-alloyed PM Steels for Optimization of Machinability and Fatigue Resistance of PM Components. J. mat. eng. Perform. (2016), pp. 764-773, DOI:10.1007/s11665-016-1900-3

Corresponding author:
Miroslava Ťavodová, Assoc. prof., MSc., PhD., +421 5206016, tavodova@tuzvo.sk

ANALYSE OF POSSIBILITIES OF USING ARTIFICIAL INTELLIGENCE FOR ENERGY CONSUMPTION PREDICTION AT SPRUCE WOOD MILLING

ANALÝZA MOŽNOSTI VYUŽITIA UMELEJ INTELIGENCIE PRE PREDIKCIU SPOTREBY ELEKTRICKEJ ENERGIE PRI PROCESE FRÉZOVANIA SMREKOVÉHO DREVA

Tomáš Čuchor[1], Peter Koleda, Patrik Gális

[1]*Technical university, Department of Manufacturing and Automation Technology (FT), Faculty of Technology, Technical university in Zvolen, T. G. Masaryka 24, 960 01, Zvolen, Slovakia, xcuchor@is.tuzvo.sk*

ABSTRACT: The aim of the article is to design and evaluate predictive models that can estimate the energy consumption of a milling operation based on predefined technological parameters chosen based on statistical results. Experimentally measured data were analysed to examine the relationship between input variables such as cutting speed, feed rate, and tool geometry, and the output variable, which is power consumption of machine. Several machine learning algorithms were applied and compared, including Artificial Neural Networks, Gaussian Process Regression, Decision Trees, Linear Regression, Kernel Regression, and Effective Linear Regression. Based on the comparison of accuracy, computational efficiency and their ability to predict the target variable with the smallest possible error rate.

Key words: energy consumption, milling, cutting parameters, artificial intelligence.

ABSTRAKT: Cieľom článku je navrhnúť a vyhodnotiť predikčné modely umožňujúce odhadnúť spotrebu energie pri operácii frézovania na základe vopred definovaných technologických parametrov, ktoré boli zvolené podľa predchádzajúcej štatistickej analýzy. Experimentálne namerané dáta boli analyzované s cieľom preskúmať vzťah medzi vstupnými premennými – ako sú rezná rýchlosť, posuv nástroja a geometria nástroja – a výstupnou premennou, ktorou je príkon obrábacieho stroja. Na predikciu boli aplikované a porovnávané viaceré algoritmy strojového učenia vrátane neurónovej siete, regresie pomocou Gaussovských procesov, rozhodovacích stromov, lineárnej regresie, Kernel regresie a efektívnej lineárnej regresie. Modely boli vyhodnocované z hľadiska presnosti predikcie, výpočtovej efektívnosti a ich schopnosti minimalizovať chybu pri odhade.

Kľúčové slová: energetická náročnosť, frézovanie, rezné parametre, spotreba elektrickej energie, umelá inteligencia

INTRODUCTION

In today's age we can't image living without items that are manufactured from wood, there are alternatives, but they are not as plentiful and cost efficient as wood. Wood and wood-based products are all around us from moment we wake to moment we go to sleep. Between raw material and final product is always several steeps, from harvesting resource in our case wood which is plentiful and renewable. There is a lot of types of wood, and every material has its technical parameters. In this study material used in experiment is spruce wood. Decision on which base was material chosen were to availability and price.

When raw material is transformed to required product, several steps must occur. In our case focus will be on woodworking machine. There are several types of machines that can transform to required parameters ranging from CNC machine centres that can create required shape with specific parameters and surface quality to simple ones like saw cutting planks in simple carpentry. Every process has parts that can be slightly improved and analysed. Tools of artificial intelligence can offer potential improvements of techniques after rigorous analysis.

This analysis can focus on challenges as tool wear, process efficiency, downtime, quality control, programming complexity and waste material.

Currently artificial intelligence offers potential as mentioned in Survey on machine learning.

There are two types of milling process monitoring, direct (offline) and the other one is indirect (online) monitoring. The offline monitoring usually uses a fiber optic sensor or charge-coupled device (CCD) camera, electric resistance, displacement, and acoustic emission, which can measure the dimensional changes in cutting tools and machined parts with high accuracy (Pasandidehpoor et al. 2025).

Real opportunity is real-time feedback control, autonomous decision making, explainability/transparency of AI in decision making, data acquisition challenges, handling variability of materials and scalability. There is also perhaps possibility or combining AI with simulation creating digital twins.

Artificial intelligence as tool that supports manufacturing has significant opportunities for overall improvement of production process. In milling process there is several opportunities for improvement with combination of CNC machining. These opportunities are ranging from creating most cost-efficient tool path, to modifying cutting parameters to conserve energy, with keeping required surface quality. That leads me to practical opportunities that artificial intelligence could bring to manufacturing such as sensor integration, data collection, model development, real time control, optimization of process planning, maintenance, tool management and quality control. As mentioned by Hirsch and Friedrich (2025) authors focused on study that explores data-driven methods, in particular deep learning, for tool wear prediction. In research by Onyegu and Mgbemena (2023) authors focused on selected milling parameters (feed, cut depth, speed) that maximize removal rate while keeping tool wear at acceptable level in order to reduce tooling costs and reduce downtime on machine. In research by Çakıroğlu et al. (2022) authors focused on surface quality and power consumption of milling process using Artificial neural networks. Their study focused on practical implications such as reduced energy costs in CNC wood manufacturing, improved surface finish consistency and enhanced decision-making in computer-integrated manufacturing systems.

The main goal of the article is to verify the possibilities of using artificial intelligence in a specific manufacturing operation, namely milling. The intention is to create a predictive machine learning model that will be able to estimate the electrical power consumption of the machining equipment based on selected technological parameters, such as cutting speed, feed rate and tool angle. Such a model will allow predicting the energy intensity of the process without the need for direct measurement, which is practical especially in cases where measurement is complicated, time-consuming, expensive or otherwise impractical.

MATERIAL AND METHODS

Measurement is done on bottom spindle moulder which is a stationary woodworking machine designed for precision shaping and profiling of wooden components. During operation, the wooden workpiece is guided along the table and brought into contact with the rotating cutter, enabling the creation of complex profiles, grooves, rebates, and joint geometries. In this process, conventional (up) milling is commonly used, where the cutter rotates against the feed direction to ensure greater control, improved surface finish, and reduced risk of tear-out—especially important when working with softwoods. Machine features a vertically mounted spindle located beneath the worktable, onto which various cutter heads can be installed. Material that is used during experiment is spruce wood with dimensions of 20 × 100

× 70 mm. The material was machined using conventional (up) milling on a bottom spindle moulder to ensure precise surface quality and dimensional accuracy.

The experiment was repeated for all combinations of technological parameters, which are listed in Table 1. Each measurement consists of the following steps:

- replacement of the milling head with the selected tool face geometry,
- setting of the cutting speed (v_c) and feed speed (v_f),
- the course of the milling process,
- recording of the power input during the entire experiment.

Table 1 Machining Parameters

Tabuľka 1 Parametre obrábania

Parameters	Values
Feed speed[1] v_f [m.min^{-1}]	6, 10, 15
Cutting speed[2)] v_c [m.s^{-1}]	20, 40, 60
Rake angle[3)]	γ = 15°, 20°
Depth of cut[4)] a_p [mm]	1

[1)]Posuvná rýchlosť, [2)] Rezná rýchlosť, [3)]Uhol čela, [4)] Hĺbka rezu

To record data on electricity consumption in real time throughout the experiment, a measurement system was set up as shown in Fig. 1. The main part is a frequency converter connected directly to a three-phase electrical network (phases L1, L2, L3). The output voltage from the converter is then fed into a sine filter, which ensures a smooth transfer of energy to the bottom spindle moulder, which serves as a machining device (Korčok, 2019).

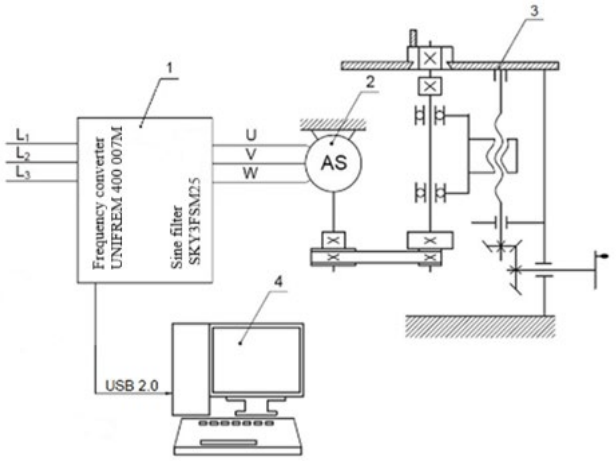

Fig. 1 Apparatus for measuring cutting power

Obr. 1 Aparatúra na meranie rezného príkonu

1 – Frequency converter UNIFREM 400 007 M with sine filter SKY3FSM25 [1)]

2 – Three-phase asynchronous motor [2)]

3 – Bottom spindle milling machine SVF [3)]

4 – Personal computer (laptop) [4)]

[1)] Frekvenčný menič UNIFREM 400 007 M so sínusovým filtrom SKY3FSM25, [2)] Trojfázový asynchrónny motor, [3)] Spodná vretenová frézka SVF, [4)] Osobný počítač (notebook)

Technical parameters of frequency converter UNIFREM 400 are shown in Table 2. Spindle miller technical parameters are shown in Table 3.

Table 2 Technical parameters of frequency converter UNIFREM 400 007 M

Tabuľka 2 Technické parametre frekvenčného meniča UNIFREM 400 007 M

M ~ quadratic load[1)]	
Motor power P_{NOM} [2)] [kW]	1,1
Rated inverter output current for quadratic load I_{NQ}[3)] [A]	3,1
M ~ constant load [4)]	
Motor power P_{NOM} [2)] [kW]	0,75
Rated inverter output current I_{NK60} [5)] [A]	2,2
Maximum inverter output current I_{NK60} [6)] [A]	3,3
Maximum inverter output current I_{NK2} [7)] [A]	4,4
Rated inverter output current I_{NIN} [8)] [A]	3,1

[1)]kvadratická záťaž, [2)]Výkon motora P_{NOM}, [3)]Nominálny výstupný prúd meniča pre kvadratickú záťaž I_{NQ}, [4)] Konštantná záťaž, [5)] Nominálny výstupný prúd meniča I_{NK60}, [6)]Maximálny. výstupný prúd meniča I_{NK60}, [7)] Maximálny výstupný prúd meniča I_{NK2}, [8)] Nominálny výstupný prúd meniča I_{NIN}.

Table 3 Technical parameters of bottom spindle miller

Tabuľka 3 Technické parametre spodnej vretenovej frézky

Parameter	**Value**
Voltage system [1)] [V]	360 / 220
Power consumption [2)] [kW]	4
Frequency [3)] [Hz]	50
Contact resistance [4)] [Ω]	0.03
Manufacturer [5)]	Maschinenfabrik Ferdinand Fromm
Year of manufacture [6)]	1976

[1)]Napäťový system, [2)]Príkon, [3)]Frekvencia, [4)]Odpor prívodov, [5)]Výrobca, [6)]Rok výroby

A typical machine learning algorithm is composed of three main components (Berkeley, 2020):

1. Decision process: a process of calculation and steps that take data and estimate what kind of pattern the algorithm is trying to find.
2. Error function: a method of measuring the quality of the estimate by comparing it with known examples. Whether the decision process proceeded correctly, if not, what the impacts of the decision were.
3. Update or optimization process: the algorithm observes errors and, based on them, updates how the decision process reached the decision and improves them in the future.

The implementation of AI in work environments leads to more efficient and cost-effective workflows. Together with the accuracy of modern AI, this contributes to the overall improvement of performance in the workplace (Duggal 2024).

Analysing often very large data sets to identify patterns can be time-consuming, financially demanding, and tiring for people. AI is simply able to identify significant trends,

uncover key insights, and recommend solutions based on processed data, which in many cases helps in making informed decisions (Duggal 2024).

The use of artificial intelligence in manufacturing is diverse and does not only concern streamlining production processes and reducing costs, but in addition to these benefits, AI also brings other benefits to companies, such as quality control, supply chain management, improving customer experience, and forecasting demand (Wuest, 2016).

The manufacturing industry needs a large logistics centre to ensure the smooth operation of the entire production process in logistics or warehouse management. The use of machine learning-based solutions helps automate various tasks associated with logistics, which leads to higher efficiency and lower costs. The average American business loses approximately $170,000 annually due to manual and time-consuming processes such as logistics or administrative tasks related to production. Repetitive tasks can be automated using machine learning, saving significant amounts of time and money. In addition, machine learning algorithms can optimize resource management – for example, Google has managed to reduce data centre cooling costs by up to 40% thanks to DeepMind artificial intelligence (ITConvergence, 2020).

Decision tree algorithms are widely used in machining because of their interpretability and low computational cost. In milling, they are often employed to predict tool wear or classify machining conditions based on features extracted from vibration, acoustic emission, and force signals. The model splits data according to critical thresholds, making it straightforward to implement in real-time monitoring. For example, a decision tree may identify chatter states or tool wear levels using vibration amplitude and spindle speed as decision nodes. Liu et al. (2022) demonstrated the effectiveness of decision tree-based models for chatter detection in milling, enabling adaptive control and stable cutting conditions (Liu et al., 2022).

Support Vector Regression is well-suited for modelling nonlinear relationships in manufacturing, particularly when data are moderate in size and precision is required. In milling, SVR has been applied to predict surface roughness and cutting force variations as a function of spindle speed, feed rate, and depth of cut. It can handle complex interactions between process parameters and machining outcomes through kernel functions, such as RBF or polynomial kernels. Natarajan et al. (2025) used SVR within an ensemble framework to predict surface roughness in polymeric machining, showing improved accuracy compared to classical linear models (Natarajan et al., 2025).

Gaussian Process Regression provides not only accurate predictions but also uncertainty quantification, which is especially valuable in high-value machining operations. In milling, GPR can predict tool wear progression and surface roughness while providing confidence intervals, enabling more reliable process planning. Because it captures correlations in data without assuming a fixed functional form, GPR is ideal for processes with nonlinear and noisy dynamics. Such probabilistic modelling supports decision-making in predictive maintenance strategies. Similar methods have been applied in tool condition monitoring to enhance reliability in smart manufacturing systems (Liu et al., 2024).

Ensemble learning methods combine multiple base learners (e.g., decision trees, SVR models) to create a more robust and accurate predictive model. In milling, ensemble algorithms such as Random Forest or Gradient Boosting have been successfully applied to predict surface roughness, detect chatter, and monitor tool wear under varying machining conditions. Wang et al. (2024) proposed an ensemble feature fusion model for tool condition monitoring, achieving high accuracy and robustness compared to single-model approaches (Wang et al., 2024). Ensemble models are particularly advantageous for handling noisy industrial sensor data.

Artificial Neural Networks have demonstrated excellent capability in capturing complex nonlinear relationships in milling processes. By processing multivariate sensor data (e.g.,

vibration, cutting forces, temperature, acoustic emission), ANNs can predict tool wear, estimate surface roughness, and optimize machining parameters in real time. Hung et al. (2020) compared ANN with classical regression models for predicting surface roughness and found that ANN provided superior accuracy and adaptability across different cutting conditions (Hung et al., 2020). Deep learning extensions further enable adaptive control and fault detection in automated milling systems.

Linear regression (LR) remains one of the most accessible and interpretable approaches for modelling machining processes, especially under stable conditions. In milling, LR has been used for quick estimation of surface roughness or cutting force behaviour when relationships between inputs and outputs are approximately linear. It serves as a baseline model for process monitoring and is easy to implement directly on CNC systems for real-time feedback. Hung et al. (2020) demonstrated that while linear regression is less accurate than ANN, it can still provide fast and practical predictions for certain machining regimes (Hung et al., 2020).

Kernel regression techniques, including RBF and polynomial kernels, enable the extension of linear regression to capture nonlinear process dynamics without the complexity of deep learning. In milling, KFR has been applied to predict dimensional accuracy, chatter onset, and surface roughness, particularly when interactions between parameters are smooth but nonlinear. Compared to SVR, kernel regression offers simpler tuning and good interpretability. Natarajan et al. (2025) demonstrated how kernel-based models enhance surface finish prediction in polymeric machining environments (Natarajan et al., 2025).

Efficient Linear Regression is a computationally optimized version of classical linear models, suitable for real-time machining control. Its low memory footprint and high-speed computation make it ideal for embedded applications such as adaptive feed rate control or on-machine tool wear compensation. While not as flexible as nonlinear models, ELR provides reliable and fast parameter estimation. This is particularly valuable in closed-loop control systems where machining forces must be regulated dynamically. Müller et al. (2023) discussed the use of efficient linear models in adaptive machining strategies for Industry 4.0 production cells (Müller et al., 2023).

RESULTS & DISCUSSION

Measured data during idle time (power during idle P_{p0}) and time with which tool is under load (power during cutting P_p) can be seen in the Fig. 2. This data from experiment were sorted to two subgroups and that is P_{p0} and P_p. Subsequently, the average value of the P_{p0} group was calculated and subtracted from each individual P_p measurement. This procedure yielded P_c (cutting power), which represents the output variable used in further data processing and analysis.

The same method was applied to all measurements obtained under different input parameter conditions. The processed data were then compiled into a comprehensive table, where each P_c value was associated with the corresponding machining parameters.

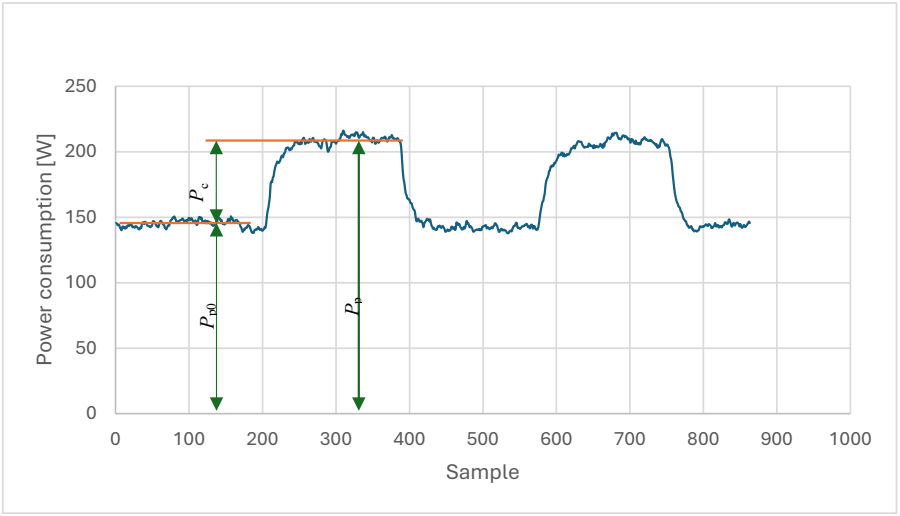

Fig. 2 Course of measured power consumption during one experiment
Obr. 2 Priebeh meraného príkonu počas jedného experimentu

Next part was statistical evaluation of data that was acquired during experiment. Statistical evaluation was done in program statistical from company TIBCO. After descriptive statistics are used to describe and summarize the characteristics of a dataset. Descriptive statistic is shown in Table 4. Dataset is then analysed using ANOVA and Duncan's test to find which factors differ between data and affect power consumption. Plot of means and confidence intervals from measured data are shown in Fig. 3.

Table 4 Descriptive statistics
Tabuľka 4 Popisná štatistická analýza

Variable	Descriptive Statistics				
	Valid N	Mean	Minimum	Maximum	Std.Dev.
Angle γ [°]	900	17,50	15,00	20,00	2,50
Cutting speed v_c [m.s^{-1}]	900	40,00	20,00	60,00	16,34
Feed speed v_f [m.min^{-1}]	900	10,33	6,00	15,00	3,68
Power consumption P	900	125,85	37,93	232,75	47,92

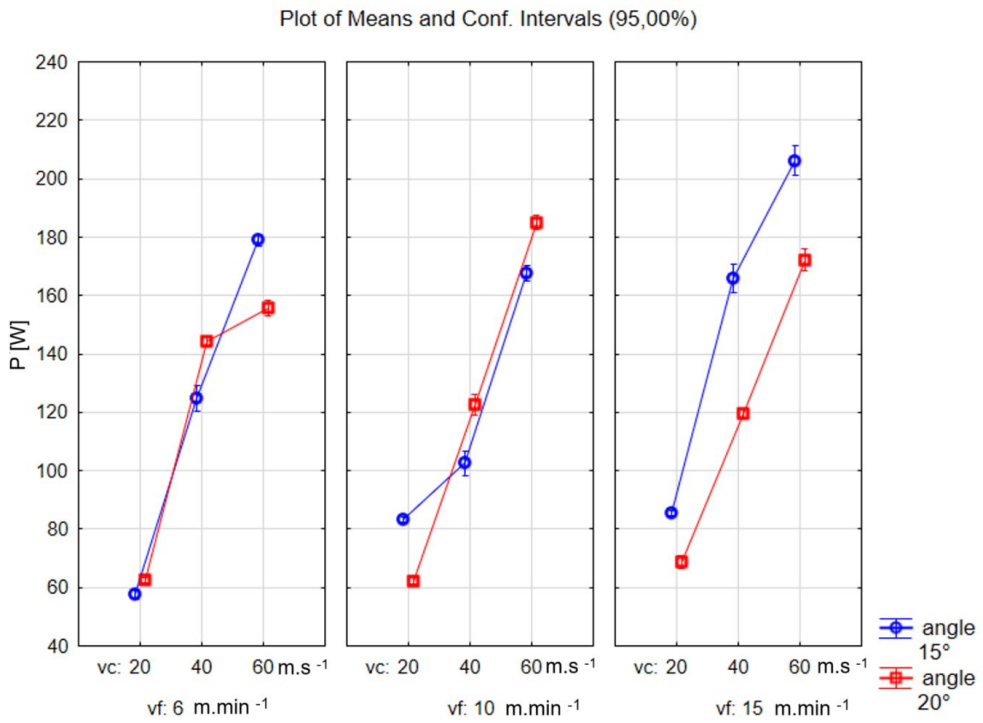

Fig. 3 Analysis of variance of measured power consumption
Obr. 3 Analýza rozptylu nameraných hodnôt príkonu

After initial processing and cleaning of the measured data, the data were imported into the MATLAB environment, specifically into the Regression Learner application. In this application, the adjusted measurement data were entered as input variables, while the target variable was the power consumption of machine during the technological operation. Next step is training all available regression models.Table Table 5 contains model name and model accuracy. Graphical interpretation is showed in Fig. 4.

Table 5 Models and their accuracy
Tabuľka 5 Modely a ich presnosť

Model No.	Model Name	Accuracy (R^2)
1	Artificial Neural Network [1)]	0.95
2	Ensemble [2)]	0.95
3	Gaussian Process Regression [3)]	0.95
4	Support Vector Regression [4)]	0.95
5	Decision Tree [5)]	0.95
6	Linear regression [6)]	0.93
7	Kernel regression [7)]	0.93
8	Effective linear regression [8)]	0.88

[1)]Umelá neurónová sieť, [2)]Kombinácia modelov, [3)]Regresia pomocou Gaussových procesov, [4)]Regresia pomocou metódy podporných vektorov, [5)]Rozhodovací strom, [6)]Lineárna regresia, [7)]Regresia s použitím jadrových (Kernelových) funkcií, [8)]Efektívna lineárna regresia

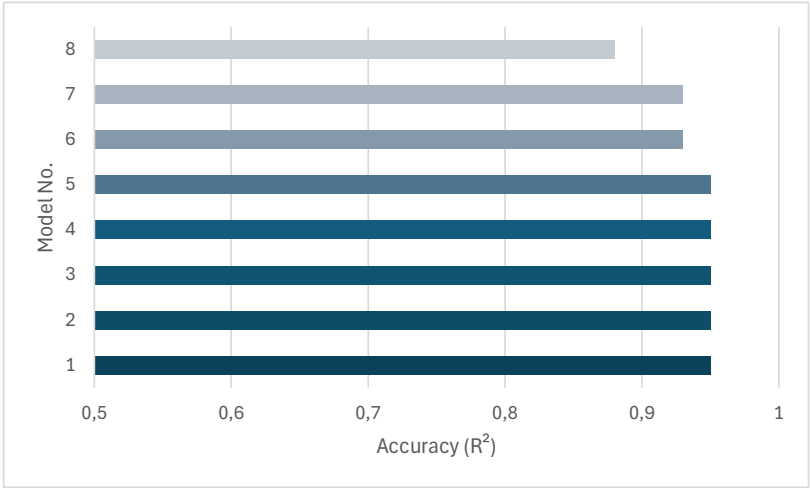

Fig. 4Prediction models with highest accuracy

Obr. 4 Predikčné modely s najväčšou presnosťou

To better illustrate the performance of the tested regression models, two representative cases were selected. The Fig. 5 shows the most accurate model, and the Fig. 6 shows the least accurate model based on the coefficient of determination (R^2) value and a visual comparison of predicted values with actual values.

These figures show the differences between predicted and actual values during the validation phase. In the case of the most accurate model, the values are distributed close to the ideal diagonal, which indicates a high degree of agreement and reliable prediction. On the contrary, significant deviations are observed in the worst model.

Such a comparison allows to point out the differences in the performance of the models in a simple and illustrative way and to justify the choice of the most suitable solution for practical use in predicting power consumption in milling.

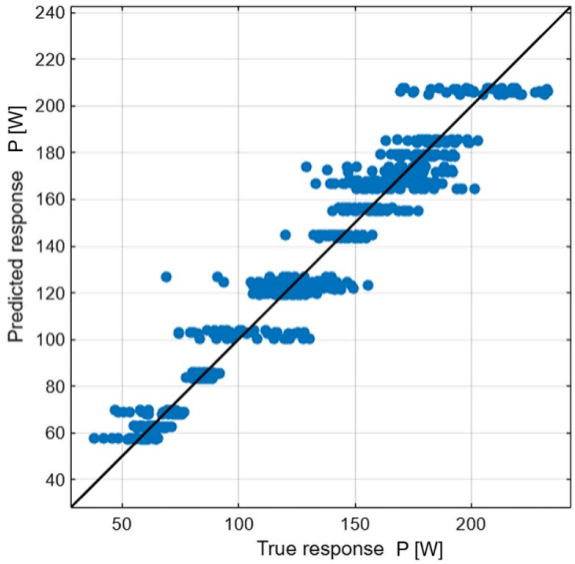

Fig. 5 Predicted and actual values comparison chart in most accurate model
Obr. 5 Porovnanie predikovaných a skutočných hodnôt v najpresnejšom modeli

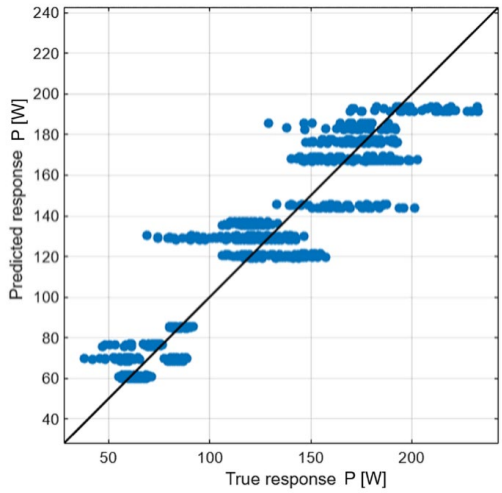

Fig. 6 Predicted and actual values comparison chart least accurate model
Obr. 6 Porovnanie predikovaných a skutočných hodnôt najmenej presný model

The selected models were further compared based on their ability to predict the target variable with the smallest possible error rate. The main indicator of accuracy was the root mean square error (RMSE). This metric allows an objective assessment of how close the predicted values are to the actual measured data. Error rate is shown in Table 6. Sorted version of graph is shown in Fig. 7.

Table 6 Root mean square error of models

Tabuľka 6 Chybovosť modelov

Model No.	Model Name	Error rate (RMSE) [W]
1	Artificial Neural Network [1)]	10,20
2	Ensemble [2)]	10,19
3	Gaussian Process Regression [3)]	10,20
4	Support Vector Regression [4)]	10,27
5	Decision Tree [5)]	10,20
6	Linear regression [6)]	12,92
7	Kernel regression [7)]	13,02
8	Effective linear regression [8)]	16,89

[1)]Umelá neurónová sieť, [2)]Kombinácia modelov, [3)]Regresia pomocou Gaussových procesov, [4)]Regresia pomocou metódy podporných vektorov, [5)]Rozhodovací strom, [6)]Lineárna regresia, [7)]Regresia s použitím jadrových (Kernelových) funkcií, [8)]Efektívna lineárna regresia

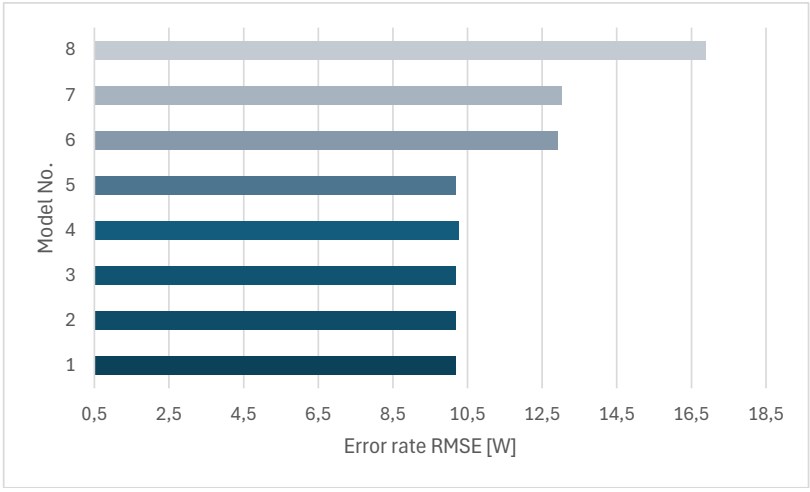

Fig. 7 Error rate of predictive models

Obr. 7 Chybovosť predikčných modelov

In addition to prediction accuracy and error rate, the time required to train a regression model is also an important factor in choosing a suitable regression model. This data is especially important in the practical application of models in production processes, where it is necessary to react quickly to changes in input parameters or data updates. Individual models were also compared in terms of computational complexity, specifically based on the time required to train them in the MATLAB environment. Time required to train in MATLAB environment is shown in Table 7. Sorted version of graph is shown in Fig. 8.

Table 7 Time of training selected models

Tabuľka 7 Čas trénovania modelov

Model No.	Model Name	Time [s]
1	Artificial Neural Network [1)]	2,93
2	Ensemble [2)]	3,06
3	Gaussian Process Regression [3)]	9,25
4	Support Vector Regression [4)]	3,09
5	Decision Tree [5)]	2,64
6	Linear regression [6)]	5,35
7	Kernel regression [7)]	7,49
8	Effective linear regression [8)]	1,08

[1)]Umelá neurónová sieť, [2)]Kombinácia modelov, [3)]Regresia pomocou Gaussových procesov, [4)]Regresia pomocou metódy podporných vektorov, [5)]Rozhodovací strom, [6)]Lineárna regresia, [7)]Regresia s použitím jadrových (Kernelových) funkcií, [8)]Efektívna lineárna regresia

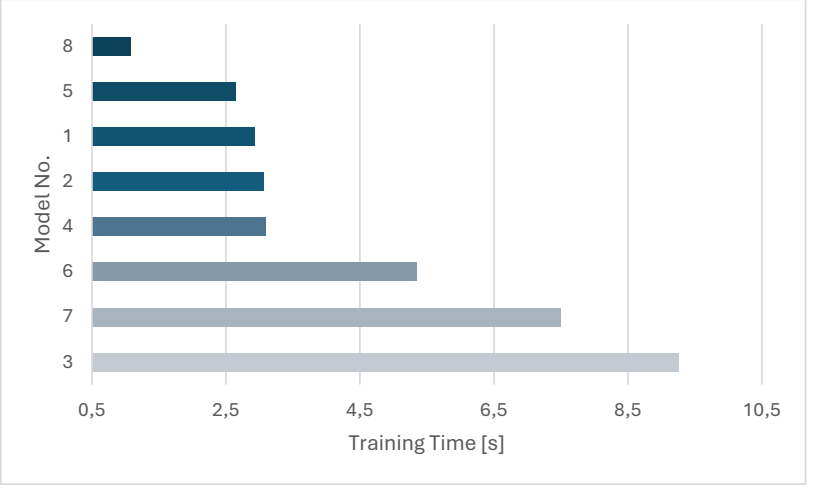

Fig. 8 Time required to train model

Obr. 8 Čas trénovania modelov

The goal is design and evaluation selected types of algorithms and choosing the most suitable one. The algorithm is chosen based on accuracy of algorithm, time required for training of data and predicted rate of error compared to data acquired during experiment. Based on Fig. Fig. Fig. andFig. , every algorithm has its strengths and weaknesses. For example, the simple linear regression model required the least amount of computing time, yet did not deliver the highest accuracy. This observation aligns with the established literature: while linear regression remains fast and interpretable, its flexibility and ultimate predictive performance are often limited compared to non-linear or ensemble approaches. As noted by Gzar et al. (2022) or Kadnár et al. (2023), linear regression exhibited low computational complexity, but also relatively lower accuracy compared to more complex models such as random forest or neural networks. Depending on size of analysed sample, computing time can be critical factor,

whereby it does not play significant role on samples of smaller size. Algorithms Artificial Neural Network, Ensemble, Gaussian Process Regression, Support Vector Regression and Decision Tree have highest predicted accuracy but differ in error rate and computational time. The choice of a particular algorithm is also influenced by the amount of data needed to supplement its learning and the need for its implementation in real time in industrial operation.

For practical implementation of real time decision making by algorithms several steps need to be taken care of, such as training data, evaluation and decision-making process. In case of decision tree requirement condition has to be chosen carefully, when choice is implemented and what impact it implements to overall process. With data that's that is evaluated and trained based on input and output parameters process can be simplified to elementary steps that algorithms can handle. It could be used in conjunction with hybrid models that offer alternative tool paths or spindle speeds. It could be simply used to check power consumption and notify algorithm or personnel in case spike occurs and or offer potential solutions for issue based on programming for personnel overseeing processes.

CONCLUSION

Based on the comparison of all tested regression models in terms of prediction accuracy, error rate and computational complexity, the decision tree was selected as the most suitable model. This model achieved high accuracy, low average error and very short training time in comparison with other models. In addition, the decision tree has the advantage of simplicity of interpretation, which is practical when implemented in a real production environment. For this reason, the decision tree was selected as the most suitable model for predicting energy consumption in milling, based on technological parameters.

ACKNOWLEDGMENT

This research was funded by APVV-20-0403 „FMA analysis of potential signals suitable for adaptive control of nesting strategies for milling wood-based agglomerates“ and the EU NextGenerationEU through the Recovery and Resilience Plan for Slovakia under project No. 09I03-03-V05-00016.

REFERENCES

BERKLEY S. of I., 2020, What Is Machine Learning (ML)?. [online]. Available at: https://ischoolonline.berkeley.edu/blog/what-is-machine-learning/.

ÇAKIROĞLU, F., KORKUT, S., & BUDAKÇI, M., 2022, Prediction of optimum CNC cutting conditions using artificial neural network models for the best wood surface quality, low energy consumption, and time savings. In *BioResources*, vol 17, 1743–1759, Available at: https://doi.org/10.15376/biores.17.2.2501-2524

DUGGAL, N., 2025, Advantages and Disadvantages of AI [online]. Available at: https://www.simplilearn.com/advantages-and-disadvantages-of-artificial-intelligence-article.

GZAR, D. A., MAHMOOD, A. M., ABBAS, M. K. 2022. A Comparative Study of Regression Machine Learning Algorithms: Tradeoff Between Accuracy and Computational Complexity. In *Mathematical Modelling of Engineering Problems*, Vol. 9, No. 5, pp. 1217-1224. https://doi.org/10.18280/mmep.090508

HIRSCH, E., FRIEDRICH, C., 2025, Data-driven tool wear prediction in milling, based on a process-integrated single-sensor approach, Cornell University available at: https://doi.org/10.48550/arXiv.2412.19950.

HUNG, J.-P., HSUEH, Y.-S., CHEN, Y.-F., 2020, Prediction of Surface Roughness Based on Cutting Parameters and Machining Vibration in End Milling Using Regression Method and Artificial Neural Network. In *Applied Sciences*, 10(11), 3941. Available at: https://doi.org/10.3390/app10113941

IT CONVENCE, 2025, 6 Benefits of Machine Learning in Manufacturing [online]. Available at: https://www.itconvergence.com/blog/6-benefits-of-machine-learning-in-manufacturing

KADNÁR, M., KÁČER, P., HARNIČÁROVÁ, M., VALÍČEK, J., TÓTH, F., BUJNA, M., KUŠNEROVÁ, M., MIKUŠ, R., BORŽAN, M. 2023. Comparison of Linear Regression and Artificial Neural Network Models for the Dimensional Control of the Welded Stamped Steel Arms. In *Machines*, Vol. 11, No. 3, p. 376. https://doi.org/10.3390/machines11030376

KORČOK, M., 2019, Analýza vplyvu technológie termicky modifikovaného dreva na energetickú náročnosť a morfológiu tvorby povrchu procesu obrábania. Dissertation thesis

LIU, Q., ZHANG, L., CHEN, S., 2024, Gaussian Process-Based Tool Wear Monitoring and Prediction for Intelligent Manufacturing. In *Journal of Manufacturing Processes*, 105, 103–112

LIU, W., WANG, P., YOU, Y., 2022, Ensemble-Based Semi-Supervised Learning for Milling Chatter Detection. In *Machines*, 10 (11), 1013. Available at: https://doi.org/10.3390/machines10111013

MGBEMENA C., ONYEGU S. O., 2023, Optimized Material Removal and Tool Wear Rates in Milling API 5ST TS-90 Alloy: AI-Driven Optimization and Modelling with ANN, ANFIS, and RSM. QEIOS, available at: https://doi:10.32388/GEGPL7.

MÜLLER, T., SCHMITT, R., SCHULZ, H., 2023, Efficient Linear Models for Real-Time Adaptive Machining. *Procedia CIRP*, 118, 234–240.

NATARAJAN, E., RAMASAMY, M., ELANGO, S., MOHANRAJ, K., ANG, C.K., KHALFALLAH, A., 2025, Ensemble Learning-Based Metamodel for Enhanced Surface Roughness Prediction in Polymeric Machining. *Machines*, 13 (7), 570. Available at: https://doi.org/10.3390/machines13070570.

PASANDIDEHPOOR, M., NOGUEIRA, A.R., MENDES-MOREIRA, J. et al., 2025, Survey on machine learning applied to CNC milling processes. *Adv. Manuf.* Available at: https://doi.org/10.1007/s40436-025-00564-x.

WANG, R., SONG, Q., PENG, Y., & LIU, Z., 2024, Tool Condition Monitoring for High Performance Milling Based on Feature Adaptive Fusion and Ensemble Learning. *Journal of Mechanical Engineering*, 60 (1), 149–158. Available at: https://doi.org/10.3901/JME.2024.01.149

WUEST, T. WEIMER, D. IRGENS, CH. THOBEN, D. K., 2016, Machine learning in manufacturing: advantages, challenges, [online]. Available at: https://www.tandfonline.com/doi/full/10.1080/21693277.2016.1192517.

Corresponding author:
Tomáš Čuchor, xcuchor@is.tuzvo.sk